Nuclear Instruments and Methods in Physics Research B46 (1990) 1–11
North-Holland

Section I. Fundamentals of defect creation

SIMULATION OF keV PARTICLE BOMBARDMENT OF COVALENT MATERIALS: AN INVESTIGATION OF THE YIELD DEPENDENCE ON INCIDENCE ANGLE

Roger SMITH * and Don E. HARRISON Jr. †

Department of Physics, Naval Postgraduate School, Monterey, CA 93943, USA

Barbara J. GARRISON **

Department of Chemistry, 152 Davey Laboratory, The Pennsylvania State University, University Park, PA 16802, USA

DON HARRISON MEMORIAL LECTURE

The dependence of the yield, Y, of ejected particles on the angle of incidence θ is investigated for the keV particle bombardment of Si by molecular dynamics simulations using many-body potentials to describe the atom/atom interactions and a Molière potential to describe the ion/atom interactions. Results are presented for the Si{110} and the dimer reconstructed Si{100}(2×1) surfaces. For Ar bombardment of the Si{110} surface at 1 and 5 keV the $Y-\theta$ curve has a number of peaks and troughs, which is a characteristic of many crystal surfaces. It is shown how the peaks and troughs can be explained by examining the interaction of the incoming ions with atoms in the surface layers. The dominant peaks in the yields as a function of incidence angle for bombardment at 1 and 5 keV are shown to agree with the shadow cone model proposed by Chang and Winograd [1]. The predictions of this model are compared with the full molecular dynamics simulations and its limitations are discussed. For the Si{100}(2×1) surface and bombardment at 1 keV, crystalline structural information was absent from the $Y-\theta$ curve whose form was characteristic of experimental measurements for amorphous Si. The calculated $Y-\theta$ curve showed some evidence of surface structure at 5 keV but the peaks in the curve could not be explained in terms of shadow cone yield enhancement.

1. Introduction

Ion bombardment in the range 100 eV to 15 keV is an important technique which is used routinely in many surface analysis methods [2]. In secondary ion mass spectrometry (SIMS) for example, the charged recoils generated by the bombardment are mass analysed in order to obtain compositional information about the surface. The bombardment process is complex and many different theoretical and computational models [3–6] have been proposed to explain how the collision cascades within the solid develop and the mechanisms for atomic ejection. Both aspects are important; the former because ions can be implanted within the solid and atomic mixing can take place which may affect the integrity of composition/depth profiles, the latter because it is information from the ejected particles which characterises the surface. The use of a mass spectrometer with ion bombardment allows surface compositional information to be obtained but recent experimental results [1,7,8] have also shown how the measured ejection yields Y, as a function of incidence angle θ, can be used to determine surface structure. The dependence of yield on incidence angle is important for reasons other than the determination of surface structure. Depth profiling in SIMS is often carried out at an angle θ_{max}, corresponding to the maximum yield in order to increase the erosion rate. It has also been shown that the form of surface topography which can develop on ion bombarded surfaces is also critically dependent on the shape of the $Y-\theta$ curve [9].

This paper presents results of molecular dynamics calculations of Ar bombardment of low index Si surfaces at different incidence angles. Molecular dynamics calculations of keV particle bombardment can predict quantitatively the energy and angular distributions of the ejected particles [3,10–13] and provide a more thorough description of ejection processes from crystalline materials than continuum [4,5] or binary collision models [6]. To date the molecular dynamics simulations have generally been carried out for bombardment of

* Present address: Department of Mathematical Sciences, Loughborough University, LE11 3TU, UK.
† Deceased 8/24/88.
** Camille and Henry Dreyfus Teacher–Scholar.

0168-583X/90/$03.50

close-packed metals. The reason for this is that the interaction potentials which model the forces between the particles in the solid have been of a form which gives the close-packed system as the preferred structural configuration. For these systems, simulations have shown that the angular distributions of ejected atoms from pure crystal metal surfaces can be explained in terms of channelling and blocking by surface atoms and these concepts have been used to determine the structure of clean [12,14] and adsorbate covered [13,15] metal surfaces. For semiconductors and valence crystals the crystal structure is more open and different interaction potentials between the lattice particles must be used in order to obtain realistic simulations. For such crystals a prescription based on radial pairwise additive forces is insufficient to model a stable lattice or account for bulk crystal properties and a many-body potential formalism must be used [16,17]. Such is the current interest in semiconductors that there have been many groups [18–28] that have independently developed many-body interaction potentials for modelling Si. The development of these potentials has recently enabled molecular dynamics simulations of keV particle bombardment to be carried out [29,30]. These simulations have been done at normal incidence and have shown that the angular distributions of ejected material are characterised by the open nature of the Si crystal rather than channelling and blocking by neighboring surface atoms as is the case for metals and that the peaks in the energy distributions of the ejected particles are higher than would be predicted by simple transport theories. The simulations have also shown that the yields of ejected material are lower than for metals. The formulation of the simulations carried out here is as described in ref. [30].

2. The molecular dynamics model

This section describes the approach used for determining the ejection yields and statistics. These are calculated using a molecular dynamics model where the interatomic forces are assumed to be derived entirely from the interaction potentials between the particles. The simulation is carried out by solving Newton's classical equations of motion treating the atoms as point particles [31]. The atoms are arranged in the regular crystal structure and the ion is aimed at different points distributed over an area characteristic of the crystal surface as a whole. The Ar/Si interactions are described by pair potentials [3,30] and the Si/Si interactions by many-body potentials [30]. Since there is no bonding between Ar and Si, the Ar/Si potential is chosen as a Molière potential. The screening length is taken as 0.80 times the Firsov value and has a cut-off distance of 3.4 Å. At close separation the Si/Si interactions are also modelled by a Molière potential but for intermediate distances there is bonding between the atoms and the Si/Si interaction is attractive. Pair potentials have been successful in simulating cascades in face-centred-cubic (fcc) metals but for covalent materials such as silicon a many-body potential formalism is used to model the crystal bonding. The results which are presented here use the Tersoff [19] formalism to describe the Si/Si interactions. This is because his potential not only gives the diamond lattice structure as the minimum potential energy configuration but it is also fit to the elastic properties and to under and over-coordinated configurations. The total potential energy E has the form

$$E = \tfrac{1}{2} \sum_{i \neq j} \left(V_{\mathrm{R}}(r_{ij}) + B_{ij} V_{\mathrm{A}}(r_{ij}) \right),$$

where r_{ij} is the distance between atoms i and j, V_{R} is a repulsive term, V_{A} is an attractive term and B_{ij} is a many-body term that depends on the positions of atoms i and j and the neighbours of atom i. This potential is not sufficiently repulsive at small distances, thus the repulsive pair part V_{R} is smoothly connected to the Molière potential with a screening length of 0.83 times the Firsov value for close particle separation. The results in ref. [30] used the second of Tersoff's potentials [18] because that was the most refined at the time the investigation was undertaken. The results presented here now use the third formulation [19] since this has better elastic properties and has been found to be more appropriate in simulations of molecular beam epitaxy [32]. The splining procedure between $V_{\mathrm{R}}(r_{ij})$ and the Molière potential has also been slightly modified. The procedure is the same as described in ref. [30] with a function of the form $\exp(ar_{ij} + b)$ where a and b are fitting constants joining the two parts of the potential between the distances $r_{ij} = r_a$ and $r_{ij} = r_b$. The original values of r_a and r_b using the second Tersoff potential [18] caused an upward shift in the Molière potential of 61 eV at r_a. The new values of $r_a = 0.353$ Å and $r_b = 0.543$ Å using the third Tersoff potential [19] give a shift of about 6 eV.

The calculations also make use of a moving atom approximation which is described in detail in ref. [30]. This approximation integrates the trajectories of only those atoms which have been sufficiently hard hit by another moving particle. If an atom in the crystal experiences a force which is less than a given threshold, then it is assumed to remain stationary. This approximation can speed up the calculations by a factor of three or more from a full molecular dynamics simulation. The same thresholds are used here as in ref. [30]. A force threshold of zero was used for the Ar/Si interactions and a threshold of 1.12×10^{-9} N for the Si/Si interactions.

4. Results

In this section the calculated Y–θ curves are presented and analysed. The peaks in the curves are compared to the predictions of the shadow cone model [1,7,8] used for determining surface structure in impact collision SIMS (ICSIMS) for both the Si{110} and {100}(2 × 1) faces. These crystal orientations are shown schematically in fig. 1 which also defines the azimuthal angle ϕ used in the text. For the Si{110} face there are two symmetry planes along the $\phi = 0°$ azimuth and these are labelled A and B in the diagram. The parallelogram drawn on the Si{110} face and the rectangle on the {100}(2 × 1) face are the representative areas over which the impact points for the ion were distributed.

The calculated yield Y, as a function of incidence angle θ, is plotted for the Si{110} face in fig. 2 for bombardment along the $\phi = 0°$ azimuth at incident energies of 1 and 5 keV. The data for each point on the plots was obtained by running 150 trajectories spread over the representative area. The size of the crystal was 631 atoms in 5 layers. Ideally more trajectories should be used to generate better statistics and a larger target should also be used but tests have shown that the calculated yields agree with a data set of 5400 trajectories run at normal incidence [30] and that the calculated yields should be statistically accurate to within 5%. At large incidence angles the was some evidence to suggest that the yields were being affected by the relatively small size of the crystal. The size of the crystal and the relatively small number of trajectories limit the angular resolution of the curves to about 1°. In this section we are primarily interested in the peaks of the yield curves and some sacrifice on accuracy was made in order to obtain data from a sufficiently large number of values within a reasonable time. Each point on the curve is equivalent to about two days computing on a 'microvax'. The results show that at 1 keV energy the yields increase by over 7.5 times at 72.5° incidence (θ_{max}) compared to normal incidence before approaching zero near grazing incidence. At 5 keV, the yield at normal incidence is slightly higher than at 1 keV but the maximum at 77.5° incidence is only just over 4 times the normal yield.

At normal incidence for 1 keV bombardment the peak in the distribution of low energy ejected atoms was at 7 eV [30]. No particle was found to be ejected with an energy > 100 eV, 88% of ejected particles were emitted

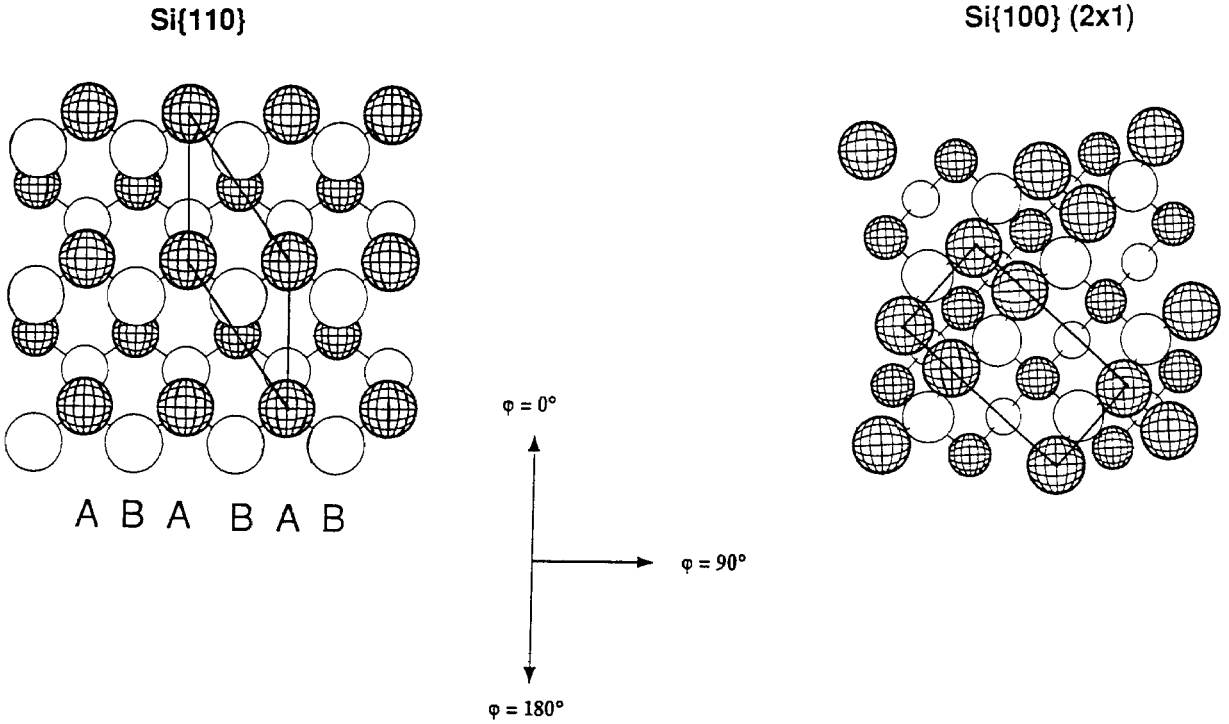

Fig. 1. The arrangement of surface atoms for the Si{110} and the dimer reconstructed Si{100}(2 × 1) surfaces. The larger circles represent top layer atoms and the circles are drawn with decreasing radii to represent depth. The hatching is for artistic purposes but could also represent the position of Ga atoms in a GaAs lattice. The azimuthal angle used in the text is described in the diagram. The A and B lettering is used to distinguish the two different symmetry lines along the $\phi = 0°$ azimuth. The outlined parallelogram and rectangle are the representative areas over which the impact points are distributed.

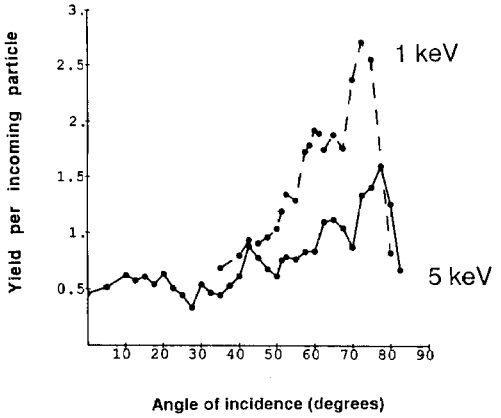

Fig. 2. The calculated yield plotted as a function of incidence angle θ for bombardment of the Si{110} surface along the $\phi = 0°$ azimuth at bombardment energies of 1 and 5 keV.

with energies less than 50 eV and 59% with energies less than 25 eV. At the incidence angle $\theta_{max} = 72.5°$, the calculated peak of the ejection energy is greater than at normal incidence. Statistics from 300 trajectories show that there is little variation in the distribution of low energy ejected atoms between about 4 and 20 eV. Analysis of the data shows that 56% of ejected particles are now emitted with energies > 25 eV and 22% with energies > 100 eV. They are also scattered preferentially in the forward direction. In a typical SIMS experiment, the particle detector will only have a small energy bandwidth and collection angle and it is important to bear in mind the contribution from the higher energy and forward recoils at oblique incidence. Measured yields may well be distorted from those presented in fig. 2 which are calculated for all energies and angles.

4.1. Impact collision SIMS

ICSIMS [1,7,8] is a new technique which has been successfully applied to determine surface structure by measuring the number of sputtered recoils in SIMS as the incidence angle varies. The technique uses a simple explanation of the peaks in the Y–θ curves to determine the relative positions of atoms in the crystal. The yields shown in fig. 2 have a number of maxima and minima as the incidence angle varies. The minima can be attributed to channelling [33] of the incoming ion. Here we test the validity of associating the maxima to the shadow cone yield enhancement mechanism. The principle of the method [1,7,8] can be described as follows. The surface atoms deflect the incident ions as they approach the crystal. The shadow cone is the area behind an atom which cannot be reached by the incoming ion. If an atom in the crystal lies in this region it does not interact with the incoming ion but if it lies just outside the edge of the shadow cone then it will experience a larger flux from incoming particles. Thus as the incidence angle varies we would expect to see a drop in the yield as the neighbouring atom comes into the region of the shadow cone, since the ion can then be injected deeper into the crystal before undergoing a collision. Alternatively if the atom lies just outside the shadow cone, particles incident from a number of different impact points would be deflected toward it, deposit their energy closer to the crystal surface and cause an enhancement to the yield. Fig. 3a illustrates the principle for the peak at $\phi = 0°$, $\theta = 60°$ for 1 keV bombardment of Si{110} shown in fig. 2. Fig. 3a shows the ion trajectories *calculated on the basis of a single collision with a surface atom* for different impact points. The relative positions of the other atoms in the crystal are also shown for one possible configuration of second layer atoms (the A plane atoms of fig. 1) although these are not included in the calculation. Fig. 3a shows that at an incidence angle of $\theta = 60°$, the surface layer atom deflects a number of ion trajectories towards a second layer atom. This causes the ion to transfer energy to this second layer atom which lies just outside the forward end of the shadow cone of the first layer atom. As the incidence angle is increased past 60°, the yield decreases due to shadowing of the second layer atom and a deeper penetration by the ion. For the single atom shadow cone technique to be successfully applied, two criteria need to be satisfied. The first is that shadow cones from adjacent surface atoms do not overlap and the second that the area of the flux concentration at the edge of the shadow cone adjacent to the atom with which the ion is interacting should be a sizeable proportion of the total ion flux crossing the plane at the depth at which the interaction takes place.

To test the validity of the shadow cone explanation, consider first calculations for the {110} face shown in fig. 2 for 1 keV Ar bombardment. There are peaks in the Y–θ curve at 60°, 65° and 72.5°. At an angle of 72.5° the forward end of the shadow cone from a surface atom intersects with another surface atom (the forward end is defined in fig. 3a). The mechanisms which give rise to the increase in the calculated yield as θ increases from 67.5 to 72.5° at 1 keV, have been examined. These show that the major part of this increase is due to the ejection of the surface atom located at the forward end of the shadow cone, giving a direct confirmation of the shadow cone yield-enhancement theory for this peak. We have already seen from fig. 3a that the forward end of the shadow cone intersects with the second layer atoms of the A plane for $\theta = 60°$ and this provides the explanation of the peak at this angle but no such simple interpretation exists for the peak at 65°. An examination of the trajectories along the two-dimensional symmetry line provides the explanation. The results in figs. 3b and 3c show that the single atom shadow cone model is only just valid at the depth of the second layer at 1 keV since the next atom along the

surface chain also plays a role in focussing the ion towards the second layer atom with which it interacts. At angles between 60° and 70° the ion trajectory is affected by two surface atoms rather than one, see fig. 3c for $\theta = 65°$. Shadow cone yield enhancement is thus only just valid to explain the second layer peak at $\theta = 60°$ and the calculations show no evidence of an expected peak at $\theta = 45°$, due to interaction with second layer B plane atoms.

The two-dimensional ion trajectories presented in figs. 3b and 3c give a good figurative description of the basis of the single atom shadow cone yield enhancement

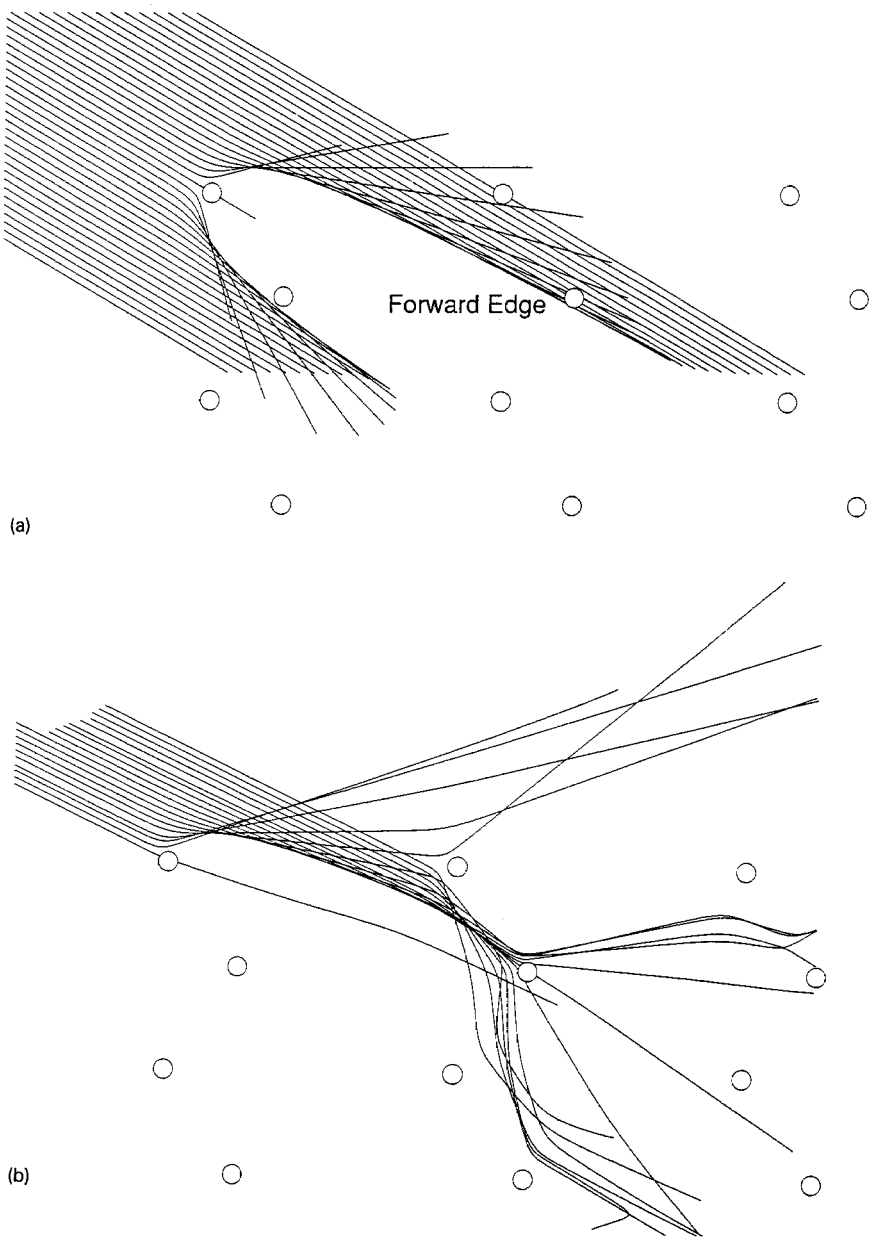

Fig. 3. A comparison between the single atom collision calculations and two-dimensional molecular dynamics simulations for 1 keV Ar^+ bombardment of Si{110} and $\phi = 0°$. (a) A cross-section of the shadow cone for a single Ar/Si collision at $\theta = 60°$ with both first and second layer atoms shown as circles. For the {110} face there are two possible arrangements of first and second layer atoms in a symmetry plane. The arrangement corresponds to the A plane atoms of fig. 1. (b) A set of molecular dynamics simulations for trajectories along the two-dimensional symmetry line corresponding to the A plane atoms of fig. 1 at $\theta = 60°$. (c) Same as (b) but with $\theta = 65°$.

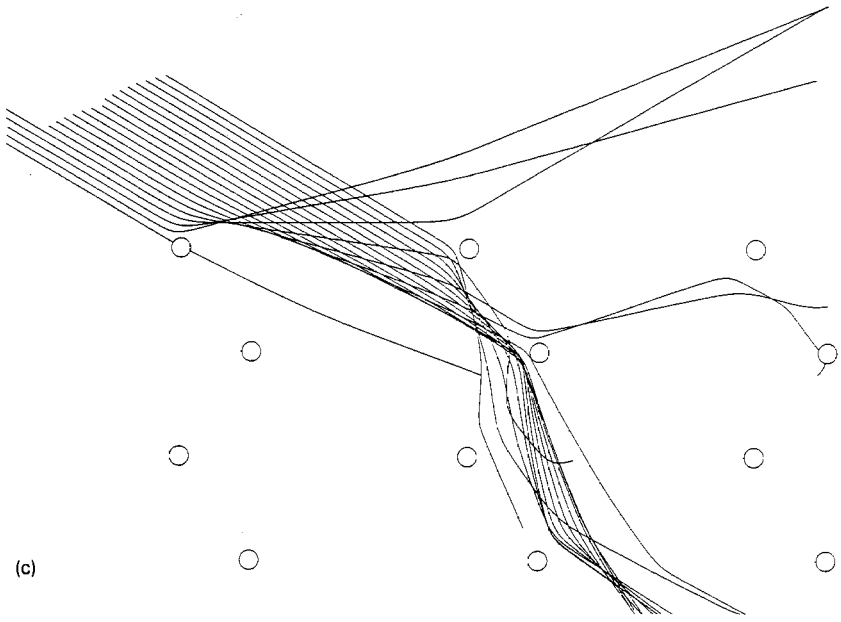

Fig. 3 (continued).

method but in practice, the trajectories are three dimensional. To illustrate the three-dimensional nature of the ion–target interactions a series of ion flux maps have been drawn at different depths. Fig. 4 shows these flux maps and compares the single atom shadow cone cross sections with the shadowing region calculated from the full dynamics. Fig. 4a shows the positions at which the ion crosses the $z = 0$ plane for $\theta = 72.5°$ and fig. 4d shows these points for $\theta = 60°$ at $z = 1.92$ Å which corresponds to the second layer of the {110} surface. Data from 4 adjacent impact zones is presented and these zones are shown outlined in figs. 4a and 4d. Figs. 4a and 4d show that the ion flux is concentrated into well-defined regions. The corresponding single atom shadow cone calculations are shown in figs. 4b and 4e and the superposition with the molecular dynamics calculations is shown in figs. 4c and 4f for comparison. The impact area for the single atom shadow cone calculations was larger than the representative area for the molecular dynamics calculations and chosen to be sufficiently large that trajectories near the edge of the impact zone undergo no deflection. It can be seen that the flux maxima (density of dots) in both cases correspond to the area just outside the shadow cone and that atomic positions lie adjacent to these areas of maximum flux. *It can be seen from fig. 4d that not all the region adjacent to the edge of the shadow cone experiences a large increase in flux.* However the concentrations of flux are adjacent to the second layer 'A' atoms. The areas of flux concentration shown in fig. 4d can be determined approximately from the moiré interference pattern produced by overlapping sets of elliptical shadow cone cross-sections. Note that in both figs. 4a and 4d there are large areas of the plane which experience very little flux and other areas which have a large concentration. *For the single atom shadow cone explanation to be valid a large proportion of all possible trajectories should be concentrated in a region adjacent to an atomic position.* If this concentration is small then other collisional effects can dominate the yield statistics and a peak in the Y–θ curve is not observed.

Because of the marginal applicability of the single atom shadow cone explanation at 1 keV, the ion energy was increased to 5 keV. At 5 keV the shadow cone has a smaller radius and ion interactions from adjacent surface atoms can be separated. Fig. 2 shows that the Y–θ curve at 5 keV has more features than at 1 keV. There are peaks at $\theta = 52°$, $65°$ and $77.5°$. All these peaks can be attributed to the shadow cone yield enhancement explanation. The peak at $77.5°$ corresponds to the forward edge of the single atom shadow cone being coincident with the adjacent surface atom and the peaks at $\theta = 52°$ and $\theta = 65°$ are due the interaction of the forward edge of the shadow cone with the second layer B plane and A plane atoms respectively. We would also expect to see a peak at $\theta = 44°$ due to interaction of the forward end of the shadow cone with the third layer atoms. There is a peak in the yield curve but this is at $\theta = 42.5°$. An examination of the ion flux maps calculated from full molecular dynamics calculations and shown at the depth of the third layer provides an explanation for the peak at $\theta = 42.5°$. Fig. 5 shows these flux maps for incidence angles of $35°$, $42.5°$ and $50°$. The incidence angles of $35°$ and $50°$ were chosen

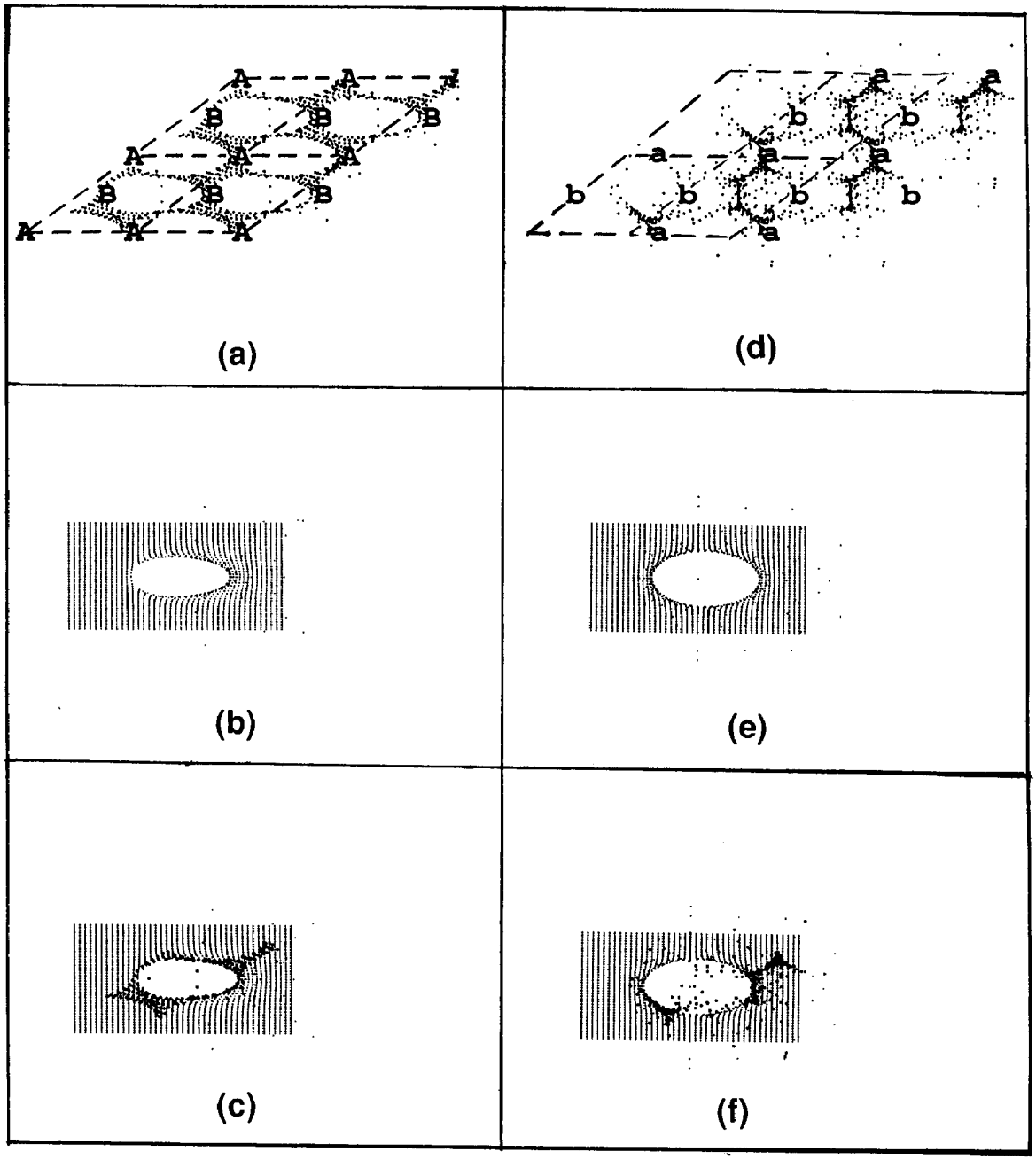

Fig. 4. A comparison between the single atom collision calculations and the molecular dynamics simulation for a set of different impact points on the Si{110} surface at a bombardment energy of 1 keV and $\phi = 0°$. Each point corresponds to where the ion trajectory crosses the z plane where z is measured perpendicular to the surface. A high density of points therefore refers to a high flux in that area. The different point sizes are used for distinguishing purposes only. (a) The ion flux at the crystal surface $z = 0$ for $\theta = 72.5°$, the calculated value of θ_{max}. The positions of the surface atoms are marked by A and B consistent with the notation for the two symmetry planes described in the caption to fig. 1. The outlined parallelograms correspond to 4 adjacent representative areas. (b) The corresponding calculation for the single atom collision. (c) The combination of (a) and (b). (d) The ion flux at a depth corresponding to the second layer, $z = 1.92$ Å and an angle of $\theta = 60°$. This value of θ corresponds to the secondmost prominent peak in the yield curve. The position of the second layer atoms are marked by a and b to represent atoms in the A and B symmetry planes as described in (a). (e) The corresponding calculation for the single atom collision. (f) The combination of (d) and (e).

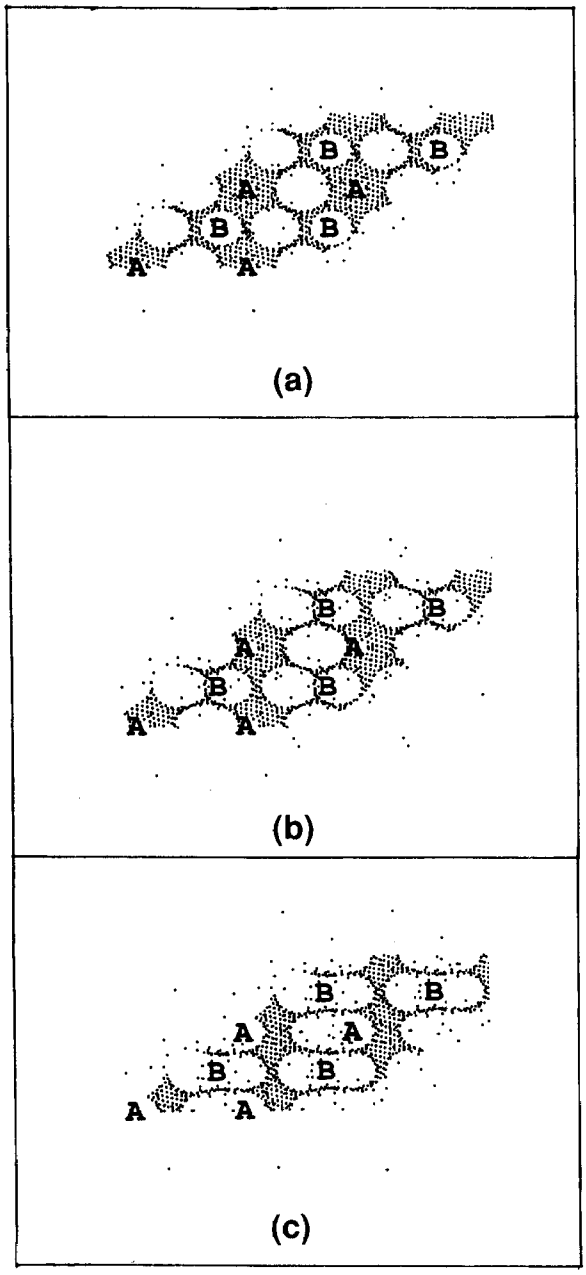

Fig. 5. The ion flux for $\phi = 0°$ and 5 keV bombardment of the Si{110} surface at a depth corresponding to the third layer, $z = 3.84$ Å and an incidence angle of (a) $\theta = 35°$, (b) $\theta = 42.5°$ and (c) $\theta = 50°$. The position of the third layer atoms are the same as those in the top layer and are marked by A and B.

because these correspond to minima in the calculated yields adjacent to the maxima at 42.5°. Fig. 5a shows that at $\theta = 35°$ a large number of trajectories are channelled by the lattice. The shadowing regions are well-defined and separated. Note that along the B plane we can clearly see two shadow regions due to ion interactions with both the first layer atoms and the second layer atoms. The third layer B atoms lie within the shadow region of the second layer atoms. Along the A plane, the second layer atoms lie in the shadow region of the first layer atoms and so do not produce their own shadow region. At $\theta = 42.5°$, the edge of the shadow regions from the first layer atoms coincide with third layer atoms in both the A and B planes but this is distorted in the B plane by deflections from the second layer atoms. As the angle of incidence increases to 50°, the shadow region from the first and second layer atoms in the B plane coalesce and include the third layer B atoms while in the A plane, the shadow region elongates to include the third layer atoms due to shadowing by second layer atoms. An explanation of both the maxima at $\theta = 42.5°$ and minima at $\theta = 35°$ and 50° in the Y–θ curves is therefore provided based only on the relative number of interactions of the ion with atoms in the third layer.

Consider now the Y–θ curve for the dimer reconstructed surface shown in fig. 6. The data for these simulations were obtained by using a target of 1280 atoms which was 12 Å deep. The chosen azimuth of $\phi = 45°$ was because the surface atoms are regularly spaced in this direction and we have shown from the simulations of the {110} surface that shadow cone yield enhancement defines a more dominant peak for the surface atoms. Thus if the model were to be appropriate for the {100}(2 × 1) face, this azimuth should be a direction in which we should see peaks due to surface atoms. The original intention was to test the general applicability of the model for determining surface structure by using the simulations to generate a set of Y–θ curves for the surface at different azimuthal angles and to use these curves and the shadow cone yield enhancement model to work back and determine the relative positions of atoms in the surface layers. However fig. 6a shows no hint of structural information of any kind and the yield curve is now representative of the shape which is indicative of amorphous materials rising to a single peak at 65° and then dropping to zero near grazing incidence. The shape of the curves are in agreement with experimental data [34] measured for amorphous Si. The peak at 65° cannot be attributed to shadow cone yield enhancement. The reason for this is that the distance between the dimer atoms along the 135° azimuth is such as to cause the shadow cones to overlap, and in addition, many trajectories pass through the surface layer undisturbed because the representative area is larger than for the {110} face.

Fig. 6b shows Y–θ curves for this surface for incident energies of 1 and 5 keV for $\phi = 90°$. The 1 keV curve again shows a form more characteristic of amorphous materials although the peak is higher than at the 45° azimuth and shifted to a slightly higher angle. The cut–off was also at a higher angle than for

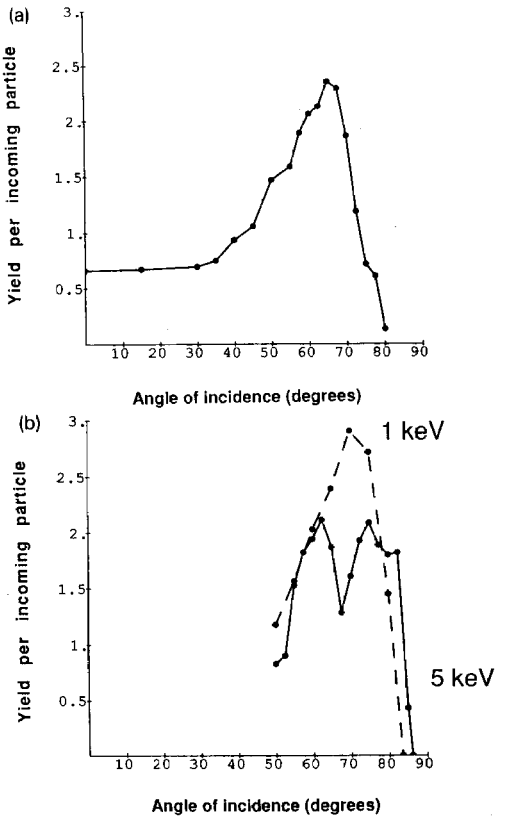

Fig. 6. (a) The ejection yield as a function of incidence angle for the Si{100}(2×1) surface at an azimuth $\phi = 45°$ under 1 keV bombardment. (b) The ejection yield as a function of incidence angle for the Si{100}(2×1) surface at an azimuth $\phi = 90°$ and energies of 1 and 5 keV.

the 45° azimuth. There are two peaks in the 5 keV curve at $\theta = 62.5°$ and 75° and a minimum at $\theta = 67.5°$. Neither peak can be attributed to shadow cone yield enhancement but an examination of the flux maps does provide an explanation. A plot of the points at which the ion trajectories cross the surface and the second layer for $\theta = 75°$ shown in figs. 7a and 7b. Fig. 7a shows the ion flux at the surface and whereas there is some flux concentration at the edge of the shadow cones this is small compared to the total amount of flux crossing the surface and is not adjacent to an atom. A large number of trajectories are unaffected by the presence of the surface atoms and thus the peak in the yield is not due to interactions with the surface atoms. At the surface, the shadow cones from the surface dimers are

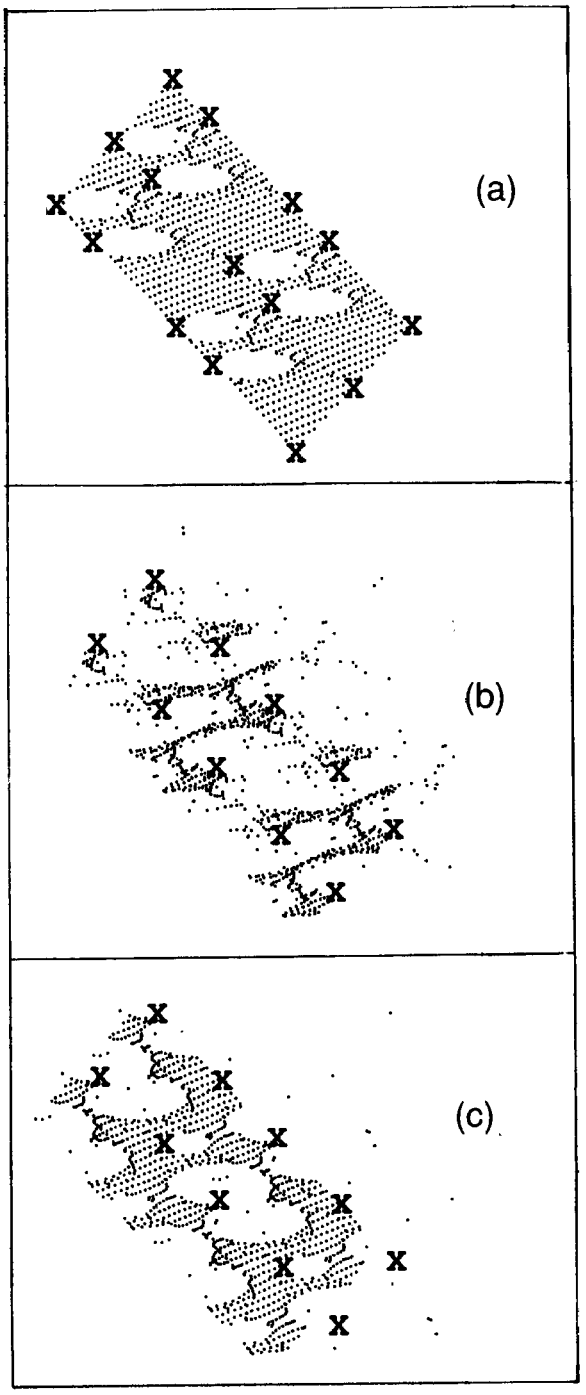

Fig. 7. The ion flux calculated from full molecular dynamics simulations for bombardment of the Si{100}(2×1) surface at 5 keV and an azimuth of $\phi = 90°$. The contribution from four adjacent representative areas is shown. (a) The flux distribution at the crystal surface for $\theta = 75°$. The crosses mark the positions of the surface atoms. (b) The ion flux distribution at the depth of the second layer for $\theta = 75°$. The crosses mark the positions of the second layer atoms. (c) The ion flux distribution at the depth of the second layer for $\theta = 67.5°$. The crosses mark the positions of the second layer atoms.

only just separated at 5 keV and overlap at the depth of the second layer. At this depth, there is some concentration of flux into certain preferred regions and these are close to atomic positions but the focussing is more random in nature than for the flux maps shown in fig. 4 and the interactions cannot be deduced from a simple single atom, collision model. For this face, an energy of > 5 keV is required to separate the focussing from the close-spaced surface atoms and allow an interpretation in terms of shadow cone yield enhancement. The ion flux is shown in fig. 7c for an angle of $\theta = 67.5°$ at the second layer. It can be seen that many more trajectories pass through the second layer undisturbed than for $\theta = 75°$ and there are no concentrations of flux next to atomic positions. It therefore appears that the peak at $\theta = 75°$ and the minimum at $\theta = 67.5°$ is due to the change in the relative number of ion collisions with second layer atoms. *These results suggest that for the technique of ICSIMS to be most effective, higher energies are required for some surfaces than those normally used in a typical SIMS experiment.* It has long been recognised [35] that an increase in bombardment energy gives an increase in the number of maxima and minima in the Y–θ curves. Experiments to measure the relative yields have generally been carried out for metals and at energies > 5 keV [35]. The simulations here have shown that for some Si crystal faces, peaks in the Y–θ curves which lead to an interpretation of the surface structure can be present at lower energies. All of the maxima and minima in the Y–θ curves examined in detail could be explained either by the simple shadow cone yield enhancement model or on the basis of the relative number of ion interactions with atoms in the surface layers.

5. Conclusions

We have examined the dependence of the yield of ejected particles on the angle of incidence using molecular dynamics simulations and tested the applicability of the shadow cone yield enhancement model used in ICSIMS. The Y–θ curves are generally complex and their form does not always have a simple interpretation. We have verified the applicability of the single atom shadow cone yield enhancement model as an explanation for some of the peaks in the Y–θ curves. For the $\phi = 0°$ azimuth of the Si{110} face, the model provides a good explanation of the main peaks for 5 keV bombardment and for some of the peaks at 1 keV. The model is simple to apply and since only a single ion/atom interaction is calculated, is inexpensive in computing time compared to the full molecular dynamics or full binary collision simulations.

For the energies and azimuths tested, the shadow cone yield enhancement model is not applicable to the Si{100}(2×1) surface. For this face the combination of a large representative area with two close-spaced dimer atoms along the $\phi = 135°$ azimuth prevent a significant shadow cone yield enhancement and at 1 keV the Y–θ curve has the same shape as for amorphous Si. At a bombardment energy of 5 keV, some evidence of structural effects is observed but the peaks in the Y–θ curves cannot be interpreted based on the ion colliding with single isolated atoms. For ICSIMS to be useful on this face, bombardment energies in excess of 5 keV would be required to separate the contributions from the dimer atoms and make the single atom shadow cone yield enhancement model applicable.

The support of The National Research Council (NPS Research Associateship) (RS), the Office of Naval Research, the National Science Foundation, the IBM Program for the Support of the Materials and Processing Sciences and the Camille and Henry Dreyfus Foundation (BJG) are gratefully acknowledged. The Naval Postgraduate School, D.D. Cleary, R.C. Olsen and X.K. Maruyama supplied generous amounts of computing time for this work. Useful discussions with D.W. Brenner, N. Winograd and R. Blumenthal were important in developing the code and understanding the results.

References

[1] C.C. Chang and N. Winograd, Phys. Rev. B39 (1989) 3467.
[2] R. Smith and J. M. Walls, in: Methods of Surface Analysis, ed. J.M. Walls, chap. 2 (Cambridge University Press, Cambridge, 1989) pp. 20–56.
[3] D.E. Harrison Jr., Critical Rev. in Solid State and Mater. Sci. 14 (1988) S1.
[4] P. Sigmund, in: Sputtering by Particle Bombardment, ed. R. Behrisch, chap. 2 (Springer, Berlin, 1981) pp. 9–71; M.T. Robinson, ibid., Chap. 3, pp. 73–144.
[5] M.W. Thompson, Philos. Mag. 18 (1968) 377.
[6] J.P. Biersak and W. Eckstein, Appl. Phys. A34 (1984) 73.
[7] R. Blumenthal, S.K. Donner, J.L. Herman, R. Trehan, K.P. Caffey, E. Furman, N. Winograd and B.D. Weaver, J. Vac. Sci. Technol. B6 (1988) 1444.
[8] C.C. Chang, G. Malafsky and N. Winograd, J. Vac. Sci. Technol. A5 (1987) 981.
[9] R. Smith, G. Carter and M.J. Nobes, Proc. R. Soc. (London) Ser. A407 (1986) 405.
[10] N. Winograd, B.J. Garrison and D.E. Harrison Jr., Phys. Rev. Lett. 41 (1978) 1120.
[11] N. Winograd, P.H. Kobrin, G.A. Shick, J. Singh, J.P. Baxter and B.J. Garrison, Surf. Sci. Lett. 176 (1986) L817.
[12] B.J. Garrison, C.T. Reimann, N. Winograd and D.E. Harrison Jr., Phys. Rev. B36 (1986) 3516.
[13] C.T. Reimann, M. El-Maazawi, K. Walzl, B.J. Garrison, N. Winograd and D.M. Deaven, J. Chem. Phys. 90 (1989) 2027.

[14] C.T. Reimann, K. Walzl, M. El-Maazawi, D.M. Deaven, B.J. Garrison and N. Winograd, J. Chem. Phys. 89 (1988) 2539.
[15] S.P. Holland, B.J. Garrison and N. Winograd, Phys. Rev. Lett. 43 (1979) 220.
[16] M. Born, Problems of Atomic Dynamics (MIT Press, Cambridge, MA, 1926).
[17] M. Born and K. Huang, Dynamical Theory of Crystal Lattices (Oxford University Press, Oxford, 1954).
[18] J. Tersoff, Phys. Rev. Lett. 56 (1986) 632.
[19] J. Tersoff, Phys. Rev. B37 (1988) 6991.
[20] J. Tersoff, Phys. Rev. B38 (1988) 9902.
[21] F.H. Stillinger and T.A. Weber, Phys. Rev. B31 (1985) 5262.
[22] D.W. Brenner and B.J. Garrison, Phys. Rev. B34 (1986) 1304.
[23] E. Kaxiras and K.C. Pandey, Phys. Rev. B38 (1988) 12736.
[24] B.W. Dodson, Phys. Rev. B35 (1987) 2795.
[25] A.D. Mistriotis, N. Flytzanis and S.C. Farantos, Phys. Rev. B39 (1989) 212.
[26] K.C. Pandey, Phys. Rev. Lett. 57 (1986) 2287.
[27] R. Biswas and D.R. Hamann, Phys. Rev. Lett. 55 (1985) 2001.
[28] M.I. Baskes, Sandia Report SAND87-8839 (Sandia National Laboratories, Albuquerque, NM 87185, 1987).
[29] R.A. Stansfield, K. Broomfield and D.C. Clary, Phys. Rev. B39 (1989) 7680.
[30] R. Smith, D.E. Harrison Jr. and B.J. Garrison, Phys. Rev. B40 (1989) 93.
[31] R. Smith and D.E. Harrison Jr., Computers in Physics 3(5) (1989) 93.
[32] D. Srivastava, B.J. Garrison and D.W. Brenner, Phys. Rev. Lett. 63 (1989) 302.
[33] D. Onderdelinden, Appl. Phys. Lett. 8 (1966) 89.
[34] S. Hosaka, I. Kanomata and S. Hashimoto, J. Vac. Soc. Jpn. 18(11) (1975) 381.
[35] H.E. Roosendaal, in: Sputtering by Particle Bombardment, ed. R. Behrisch, chap. 5 (Springer, Berlin, 1981). pp. 219–256.